Elastocaloric effect: Impact of heat transfer on strain-induced crystallization kinetics of natural rubber

Hiba Haissoune, J.-M. Chenal, Laurent Chazeau, Gaël Sebald, Isabelle Morfin, Laurent Lebrun, Florent Dalmas, Gildas Coativy

Elastocaloric effect: Impact of heat transfer on strain-induced crystallization kinetics of natural rubber

Hiba Haissoune[a,b], Jean-Marc Chenal[b], Laurent Chazeau[b], Gaël Sebald[c], Isabelle Morfin[d], Laurent Lebrun[a], Florent Dalmas[b], Gildas Coativy[a]

[a] Univ Lyon, INSA-Lyon, LGEF, EA682, F69621, Villeurbanne, France
[b] University Lyon, INSA-Lyon, CNRS, MATEIS, UMR 5510, F69621 Villeurbanne, France
[c] ELyTMaX IRL3757, CNRS, Univ Lyon, INSA Lyon, Centrale Lyon, Université Claude Bernard Lyon 1, Tohoku University, Sendai, Japan
[d] Univ. Grenoble Alpes, CNRS, LiPhy, F-38000 Grenoble, France

Corresponding author: gildas.coativy@insa-lyon.fr

Abstract:

When natural rubber is rapidly loaded and unloaded there occurs a variation of its temperature called the elastocaloric effect. The objective of this work was to determine whether this temperature variation could be responsible for a delay in strain-induced crystallization (SIC) kinetics and stress relaxation. To this end, the SIC kinetics of cross-linked natural rubber samples with different thicknesses was studied at constant elongation after adiabatic stretching using thermal, mechanical and *in-situ* WAXS characterizations. The coupling of these techniques revealed that, at a fixed elongation λ (between 5 and 6), the crystallization kinetics and stress relaxation were faster in the thinner sample (with a short heat exchange time constant), thus providing evidence that heat transfer affected the SIC kinetics and should be considered when interpreting experimental results.

Keywords: Natural rubber, Strain-induced crystallization, Crystallization kinetics, Latent heat, Infrared camera.

1. Introduction

The elastocaloric effect (eC) in elastomers can be used as an alternative cooling technology that has the potential to be cheap, efficient and environmentally friendly.[1–3] This effect is known as the change in temperature of a material when subjected to cyclic mechanical solicitation. It has been observed in different elastomers such as Natural Rubber (NR)[4–7] , blends using recycled Natural Rubber[8], Polyurethanes [9,10], Silicone, Styrene-Butadiene[11] and poly(styrene-bethylene-co-butylene-b-styrene) (SEBS)[12]. In the following study, we focus on NR which has a large temperature variation up to ΔT=12°C and good fatigue resistance[3]. The origin of its eC effect is Strain-Induced Crystallization (SIC) and entropic elasticity.[7,8,11] Since the SIC is not an instantaneous phenomenon [13–15], its kinetics will necessarily have an impact on the choice of the operating frequency of the elastocaloric device, hence the need to study it. Among the first investigations carried out on the subject, one can cite that of Mitchell and Meier [16] who showed, using thermal measurements, that the crystallization of NR started less than 50 ms after the adiabatic deformation. More recently, this result was confirmed by Candau et al [17] and Albouy et al [18] based on *in-situ* WAXS measurements. The same technique was employed by several authors to demonstrate that at constant elongation, the crystallization kinetics could last several tens of seconds, [13–15,19–21] and this observation has been explained by mechanisms based on polymer chains diffusion, crystal nucleation and stress relaxation [13–15].

These results suggest that in order to maximize the phase transition at the origin of the elastocaloric effect, it would be preferable to perform long-period cycles (at least one hundred seconds). However, from an elastocaloric point of view, lowering the frequency would limit the power involved, which is why it would seem relevant to increase the frequency as much as possible. However, in this case, the material would partially crystallize and the heat that can be exchanged during the cycle between the system and the surroundings would be limited. In addition, the average temperature of the sample at high frequency can increase considerably due to self-heating (because of the viscoelasticity of the material) [17] and might reach 50°C at 70Hz. According to the literature [7,10], with such an increase in temperature, the crystalline fraction developed at a given elongation would decrease considerably ($\frac{d\chi_c}{dT} = -0.5\%/°C$) [19] thus restraining the eC effect.

Crystallization kinetics is also temperature-dependent since it is controlled by the nucleation rate [15,23,24] which in turn is affected by the energy barrier that must be crossed

to create nuclei. In fact, when NR is stretched adiabatically at high elongations, crystallization is favored by the high elongations but the temperature rise induced by this phase transition (up to 12°C at λ=6) [4,25] is likely to hinder the nucleation process as long as the generated heat has not been totally evacuated to the external environment. For a sample with an initial thickness equal to 1 mm that is stretched adiabatically at λ=6, the time required to reach thermal equilibrium with the air is of the order of a few tens of seconds [26,27]. This also corresponds to the duration of the fast relaxation induced by crystallization [28], and thus the following question arises: to what extent does heat transfer have an impact on the strain-induced crystallization kinetics?

In this work, the crystallization of an industrial crosslinked NR was characterized by *in-situ* Wide-angle X-ray Scattering (WAXS) and Infra-Red (IR) thermography at different elongations in order to study the correlation between the duration of the crystallization process and the time needed to exchange the generated heat with the surroundings. We prepared crosslinked NR samples with different thicknesses (between 0.13 mm and 1.15 mm) but identical intrinsic properties, so that only their form factor varied and thus also their heat exchange time constant τ (a parameter characterizing the heat exchange between the sample and its surroundings [29]). In order to maximize the potential influence of the increase in temperature during the test on the crystallization, samples were stretched under adiabatic conditions. Finally, the impact of heat transfer on the crystallization kinetics was discussed.

2. Experimental setup

2.1 Materials and specimen geometry

Two types of unfilled crosslinked natural rubber samples were studied in this work. The first one, denoted $NR_{1.53}$, was purchased from Xinyinte Rubber Products Co., Ltd., China and the second, named $NR_{1.46}$, was prepared in the laboratory using the recipe detailed in Table 1. The densities of the elastically active chains (EAC) of these materials were estimated from the swelling ratio in toluene and from the Flory-Rehner equation [30] and were found to be $1.53 \times 10^{-4}\, mol.cm^{-3}$ and $1.46 \times 10^{-4}\, mol.cm^{-3}$, respectively. This EAC density was high enough to avoid undesirable phenomena (inverse yield, stable crystals at room temperature after retraction[31–33], …) and close to the optimal EAC density that would allow a maximum crystallization rate [34].

Table 1: Chemical composition of the studied material in phr (parts per hundred, i.e., g per 100g of rubber)

Components	$NR_{1.46}$
NR	100
6PPD*	3
SA**	2
ZnO	1.5
CBS***	1.9
Sulfur	1.2

*N-(1,3-dimethylbutyl)-N′-phenyl-p-phenylenediamine), **Stearic acid, *** N-cyclohexyl-2-benzothiazole sulfenamide.

Regarding the geometry of the samples, the original length was 40 mm with an initial distance between the jaws of 20 mm, and a width of 20 mm. The thickness of $NR_{1.53}$ was 0.63 mm, and those of $NR_{1.46}$ were 0.19 mm and 1.15 mm.

2.2 Mechanical measurements

The tensile testing machine was similar to the one used by Yoshida et al. [35]. It is a single axis robot RSDG212 (MISUMI Corporation, Japan) with an analog force sensor XFTC300-200N (Measurement Specialties, France). The displacement was measured via a Laser optical displacement sensor ILD1420-200 (micro-epsilon, France). The signals recovered from both sensors were simultaneously recorded via an oscilloscope.

In order to avoid residual elongation due to Mullin's effect [36] and to ensure reproducibility of thermomechanical properties, the material was subjected to cyclic strain (between $\lambda = 1$ and $\lambda = 6.8$) ten times. The initial length was then adjusted in order for the sample to be taut. The samples were tested at least 5 minutes after this procedure, and the same waiting time was applied between each test at room temperature (i.e. T=22°C). It was indeed checked that 5 min was enough for the materials to show the same mechanical response as a material having rested during 30 min (cf. supporting information Fig.S1; note that 5 minutes would be likely insufficient in the case of a filled elastomer). The distance between the jaws was taken as the initial length l_0 and the elongation was defined as $\lambda=\frac{l(t)}{l_0}$.

2.3 Thermal measurements

While stretching the material, an infrared camera, Optris PI450 (Optris, Germany) with a 29° optic simultaneously recorded the temperature variation of its surface. The frequency chosen to acquire the signal was f=80 Hz and the surface of measurement was about 15 mm^2.This surface was chosen to be in the center of the material in the stretched state to minimize the effect of the edges (both mechanically and thermally). A second area was used to measure the temperature in the center of the material at λ=1. (see Supporting Information Fig.S.2)

During the test, there were three possibilities for the sample to evacuate thermal energy: thermal radiation, heat conduction with a clamping system, and convection. The former was neglected since the temperature variation between the sample and the environment remained small (up to 13K at most). The second was also neglected since the thermal conductivity of NR is small (~0.146 $W.m^{-1}.K^{-1}$) [37], and also because the jaws were covered with strips of natural rubber acting as thermal insulators. An emissivity of 0.95 was used during our experiments [38], in accordance with a comparison between direct measurements using a thermocouple and the information retrieved by the IR measurements. Convection was considered to be the most important mechanism of heat exchange.

2.4 *In-situ* WAXS measurements

The *in-situ* WAXS measurements were carried out on the D2AM beam-line of the European Synchrotron Radiation Facility (ESRF). The X-ray wavelength was 1.54 Å. The irradiation area was about 150*150 μm^2. The acquisition times were fixed at 500 ms for the part of the study dedicated to the characterization of the crystallization right after deformation, and this time was then extended to 5 s to study the evolution of the crystallinity index during 200 s after adiabatic stretching. Each pattern was integrated as a function of the scattering angle (2θ), cleaned of air scattering, and then normalized by sample thickness and transmission.

In this study, the evolution of the crystallinity was followed via the intensity of the (200) plane's reflection after the deconvolution of the curve I=f(2θ) (denoted I_{200} and proportional to the crystallinity index as shown in Supporting Information, Fig.S3). This intensity will be called crystallinity index since it does not correspond to the real value of crystallinity.

3. Results and discussion

The impact of heat transfer on strain induced crystallization kinetics is expected to be maximal when sample is stretched adiabatically. Therefore, to determine the adiabatic and isothermal deformation domains, $NR_{1.53}$ sample was deformed at different strain rates ranging from 0.005 s^{-1} to 16 s^{-1} between λ=1 and λ=7. The maximum temperature variation measured after discharge $|\Delta T_2|$ are plotted in Fig. 1 as a function of the strain rate ($d\lambda/dt$). The results suggest that at high rates of deformation ($d\lambda/dt > 8\ s^{-1}$) the temperature change is almost constant (≈ 13°C) (adiabatic domain). Once this strain rate is lowered, the sample exchanges heat with the external environment, therefore the values of $|\Delta T_2|$ gradually decrease until reaching 0°C at $d\lambda/dt = 0.005\ s^{-1}$ indicating entry into the isothermal domain.

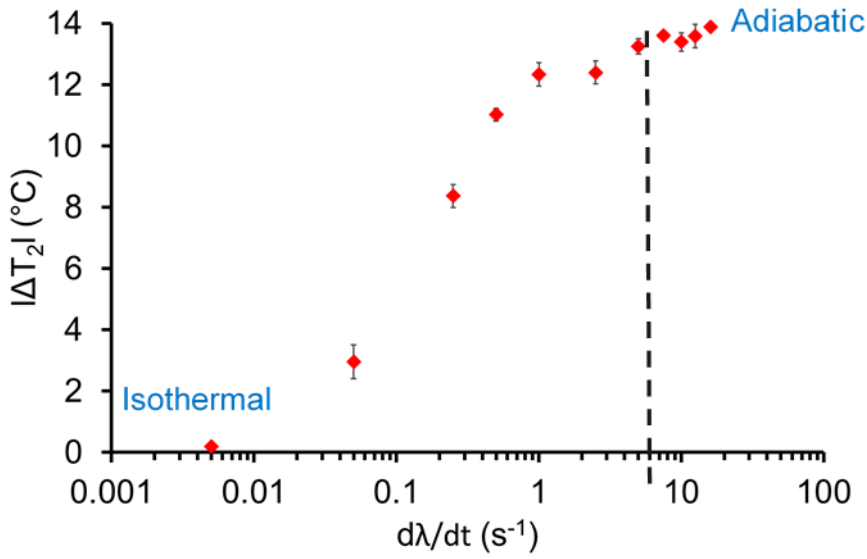

Fig. 1: Temperature variation measured after retraction (ΔT_2) at different strain rates between 0.005 s^{-1} and 16 s^{-1} for $NR_{1.53}$

The $NR_{1.53}$ sample was stretched under adiabatic conditions at a strain rate of 16 s^{-1}, from $\lambda = 1$ to $\lambda_{max} = \{4.5; 5; 5.5; 6; 6.5\}$ and then maintained at constant elongation for 200 s before returning to $\lambda = 1$ as shown in Fig. 2-a. The step of the mechanical program which occurs at constant elongation will be called holding step. The corresponding temperature change profiles are given in Fig. 2-b and the stress-elongation curves are plotted in Supporting Information, Fig.S4.

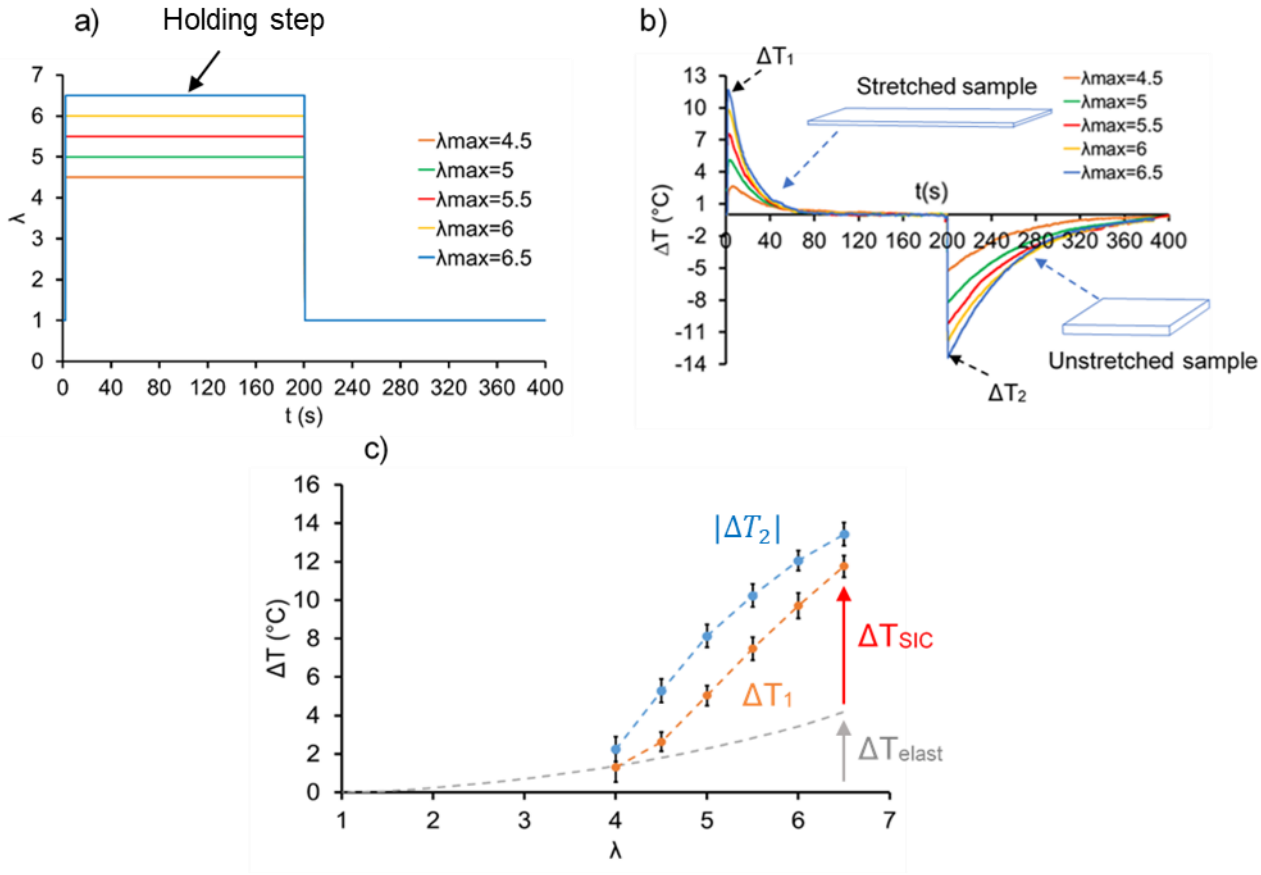

Fig. 2: a) Mechanical loading conditions: the $NR_{1.53}$ sample with a thickness of 0.63 mm was stretched to different maximal elongations λ_{max} between 4.5 and 6.5 at $\dot{\lambda} = 16\ s^{-1}$; b) Corresponding temperature changes profiles ($\Delta T=T_{measured}-T_{room}$); c) Adiabatic temperature variations after loading (ΔT_1) and unloading ($|\Delta T_2|$) (blue and orange dots, respectively) as well as the entropic contribution $\Delta T_{entropic}$ (grey dashed line)

Firstly, while stretching the sample, a positive temperature variation ΔT_1 was measured. It resulted from the entropic elasticity and the strain-induced crystallization (SIC) [6,16]. A negative temperature variation ΔT_2 was observed when the sample was unloaded after heat exchange and its absolute value increased with the elongation. This cooling effect was due to the melting of crystallites and to entropic elasticity recovery [6].

The second observation was related to the kinetics of heat exchange. For each elongation, the area under the peak ΔT_2 presented in Fig. 2.b was much wider than the one under the peak ΔT_1. Indeed, when the sample was stretched, its thickness decreased and its exchange surface became larger [26] wherefore the convective heat flow φ increased as well. The small thickness of the sample also helped reduce the thermal gradient within the thickness of the rubber films. The Biot number remained below 0.1 in all the experiments (Bi=hL/k, where h is surface heat exchange coefficient ~12W.m^{-2}.K^{-1}, L is the thickness of the samples which is

inferior to 1.15 mm for each experiments, and k is the thermal conductivity of natural rubber ~0.15 $W.m^{-1}K^{-1}$). Therefore, the temperature of the NR film may be considered as uniform, and the heat flow φ across the external rubber surfaces may be linked directly to convection via the difference in temperature with the ambient temperature ΔT:

$$\varphi\,(t) = h \times S(\lambda) \times \Delta T(t) = \frac{\rho \times C_m \times V}{\tau\,(\lambda)} \times \Delta T(t) \qquad (1)$$

Here, $S(\lambda)$ is the external surface of the sample, ρ the density, C_m the heat capacity, V the volume and $\tau\,(\lambda) = \frac{\tau\,(\lambda=1)}{\sqrt{\lambda}}$ the heat exchange time constant at a certain elongation λ [29]. In turn, $\tau\,(\lambda = 1)$ is the time needed for the sample to absorb 63% of the heat from the surroundings to reach the ambient temperature at λ=1. This value was directly determined from the second part of the temperature profile by analogy with the time constant of a first-order system, and was found to be (52 ± 5) s for $NR_{1.53}$ and $(92\pm6)\ s$ for $NR_{1.46}$.

Fig. 2.c includes the total temperature changes measured after stretching ΔT_1 and retraction $|\Delta T_2|$ as well as the contribution of entropic elasticity ΔT_{elast} which is assumed to be proportional to the volumetric work given to the sample during adiabatic loading ($W_{loading}$), as mentioned by Mitchell et al [16]:

$$\Delta T_{elast} = \frac{W_{loading}}{\rho \times C_m} \qquad (2)$$

These three temperature variations increase from ΔT_1 = 1.3°C, $|\Delta T_2|$ = 2.2°C and ΔT_{elast} = 1.3°C at λ=4 to ΔT_1 = 11.7°C, $|\Delta T_2|$ = 13.3°C and ΔT_{elast} = 3.8°C at λ=6.5. This difference between the temperature variation values after loading and unloading reflects the fact that during retraction, the number of crystallites that melt is greater than that created just after stretching. This result comes from the existence of kinetics of crystallization which is responsible for the increase of the crystallinity index χ(t) during the holding step. The previous thermal measurements made it possible to describe the crystallinity index as a function of time using an equation similar to the one proposed by Plagge. [39] The main difference is that we fix the term which multiplies $(T(t) - T_{room}(t)) * \sqrt{\lambda(t)}]$ (equ3) and do not consider it as an adjustable parameter. In the work of Plagge et al. the adjustment is done in order to assure that crystallinity is null at λ=1.

$$\chi(\mathrm{t}) = \int_{\mathrm{t_0}}^{\mathrm{t}} \frac{\mathrm{C_m}}{\tau(\lambda)*\Delta \mathrm{h_f}} (\mathrm{T(t)} - \mathrm{T_{room}}(t))\mathrm{dt} + \frac{\mathrm{C_m}}{\Delta \mathrm{h_f}} \left(\mathrm{T(t)} - \mathrm{T_{\lambda_f}}\right) + \frac{\mathrm{C_m}}{\Delta \mathrm{h_f}} \left(\Delta \mathrm{T_{\lambda_f}} - \frac{W_{loading}}{\rho \times C_m}\right) \qquad (3)$$

Here, t_0 is the moment when the maximal elongation λ_{max} is reached , ρ=910 kg/m^3 the density

[40], C_m = 1900 J/(kg.K) the heat capacity [16], $\tau(\lambda)$ the heat exchange time constant, T the measured temperature, T_{room} the room temperature, T_{λ_f} the temperature reached just after elongation and Δh_f = 64 J/g the melting enthalpy [4].

All the results obtained via equation (3) during the holding steps at different elongations are presented in Fig. 3.a. Firstly, for each test, the index of crystallinity increases with elongation and tends to stabilize to a maximum (χ_{max}) when the temperature no longer changes after a specific time that depends on the maximal elongation λ_{max}. The lowest χ_{max} (8% for λ_{max} =4.5) is reached after 100 s and the highest one (24% at λ_{max} = 6.5) after 70 s. These durations coincide with the time needed to evacuate all the heat generated after loading (5τ: indicated in Fig. 3.a by black stars).

To verify that this slowdown of kinetics is not dependent on the employed method used, the evolution of the crystallization was characterized by WAXS using a synchrotron source. The intensity I_{200} diffracted by the (200) plane was followed during the holding step at different maximal elongations between 5 and 6.5. It was not possible to do the same for λ_{max}=4.5 because the low level of crystallinity reached, made detection too difficult with this technique. The time at which the acquisition started was however increased at 1 s after the deformation (instead of 0.1 s for the thermal acquisition), because of the minimum acquisition time of the X-ray patterns (around 500 ms).

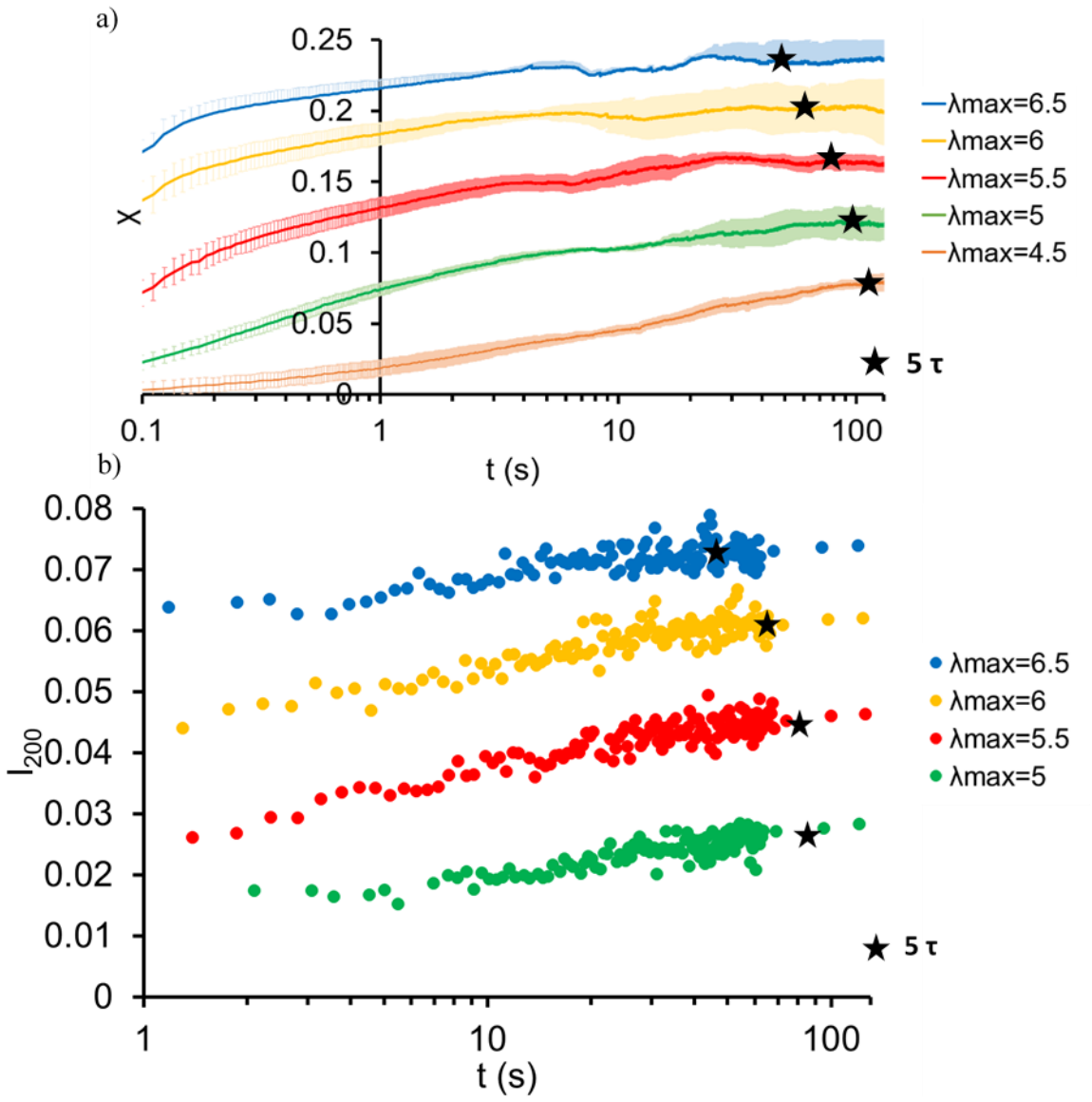

Fig. 3: Evolution of (a) the crystallinity index determined using eq (3) and (b) the intensity of (200) planes diffraction measured via WAXS in $NR_{1.53}$ during the holding steps at different elongations as a function of time after fast stretching at $\dot{\lambda} = 13\ s^{-1}$ (5τ corresponds to $\frac{5*\tau\ (\lambda=1)}{\sqrt{\lambda}}$)

As can be seen in Fig. 3.b, the intensity I_{200} evolves significantly during tens of seconds (black stars added on each curve of the same figure) and then slower after. This duration also corresponds to the time needed to evacuate the heat generated after adiabatic stretching (as presented on Fig 2.b). These results therefore suggest the existence of a link between the crystallization kinetics and the heat exchange which will be studied in more detail in the next experiment.

$NR_{1.46}$ samples with two thicknesses (0.19 mm and 1.15 mm) were prepared in order to vary the characteristic heat exchange time constant $\tau(\lambda)$. It decreases from (92±6) s to (20±3) s when the thickness is reduced from 1.15 mm to 0.19 mm (Figure S.5). Subsequently, two main physical quantities were used to study the evolution of crystallinity during the holding step: stress and I_{200} intensity. Fig.4 shows these quantities for $NR_{1.46}$, at constant elongation λ=6. It clearly evidences that stress relaxation occurs faster for the thin sample for times lower than 70s and with the same kinetics for times longer. Regarding the I_{200} intensity, it increases faster for the thin sample during the first 70s.

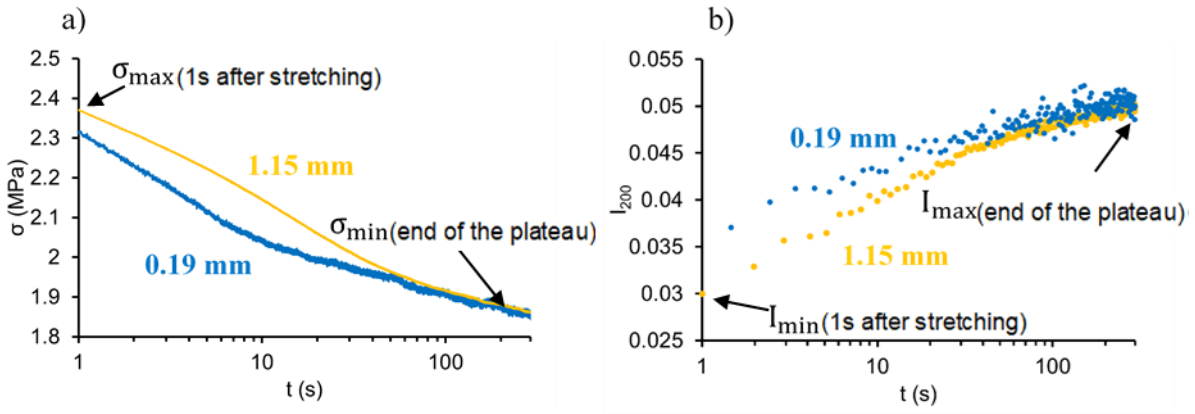

Fig. 4: a) Stress (σ) and b) Intensity I_{200} of X-ray Diffraction during the holding step at λ=6 as a function of the time for two sample thicknesses: 0.19 mm and 1.15 mm of $NR_{1.46}$ after fast stretching at $\dot{\lambda} = 13\ s^{-1}$

It is difficult to compare stress and I_{200} intensity directly since the stress decreased whereas the intensity increased. Consequently, their variations were compared using two indices.

The first index was calculated via equation (4) and is presented in Fig. 5. It is based on the stress relaxation, and related to the SIC as shown by Flory [41]:

$$\frac{\Delta\sigma(t)}{\Delta\sigma_{max}} = \frac{\sigma(t)-\sigma_{min}}{\sigma_{max(1s\ after\ stretching)}-\sigma_{min}} \quad (4)$$

were σ_{max} is the maximum stress 1s after loading and σ_{min} is the stress reached at the end of the holding step.

From 1s to 70 s after deformation, a large difference is found between the stress curves (continuous lines) of thick (1.15 mm) and thin (0.19 mm) samples. This trend was also observed on the same specimen with other thicknesses (0.13 mm and 0.34 mm) and on another material

($NR_{1.53}$) (see supporting information, Fig.S6). The results show that the thicker samples relax more slowly, likely due to slower crystallization kinetics. The largest relative difference (40%) is observed at about 8 s after deformation. Beyond 70 s, all curves merge indicating that both samples have the same crystallization behaviors when the heat exchange ends. However, the stress does not appear to be stabilized at the end of the time interval studied, probably because the crystallization continues to evolve very slowly over a longer duration than the one of our study or because of viscoelastic effects [9,17]. This points at the fact that stress relaxation is not completely driven by the heat exchange, and that it may also be related to the relaxation of the amorphous phase which decreases the local elongation and delays the SIC [15].

The relative evolution of the stress relaxation was then compared to that of the intensity of the peak 200 (square symbols) calculated via equation (5):

$$\frac{\Delta I_{200}(t)}{\Delta I_{200_{\max}}} = \frac{I_{max} - I(t)}{I_{max} - I_{\min(1s\ after\ stretching)}} \quad (5)$$

The results of this comparison displayed in Fig. 5 show a good correlation between the evolution of the stress relaxation and the intensity for both thicknesses. The modelling of stress relaxation using a modified model of Flory supports also these results (Fig.S.7). Furthermore, they confirm that the crystallization kinetics is faster in the thinner sample. This suggests that the heat generated by SIC and entropic elasticity, could significantly delay the crystallization kinetics of the thicker sample.

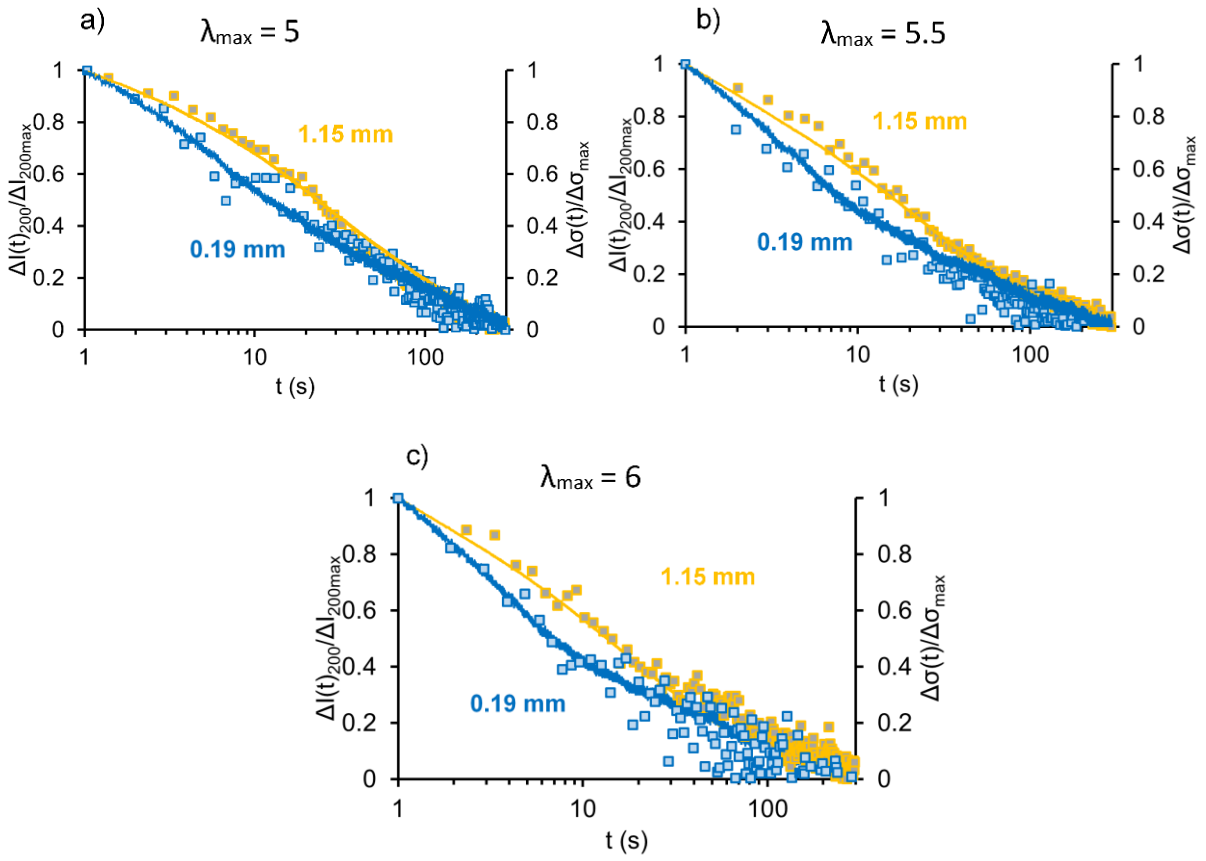

Fig. 5: Stress relaxation (solid lines) and intensity variation (squares) during the holding step (after rapid stretching $\dot{\lambda} = 13\ s^{-1}$) for the thicknesses 0.19 mm (blue) and 1.15 mm (yellow) at three final elongations: (a) λ=5, (b) λ=5.5 and (c) λ=6.

It is generally admitted that SIC is governed by the successive nucleation of crystallites (characterized by their dimensions). Their appearance depends on the spatial heterogeneous distribution of the topological constraints resulting from the successive appearance of the crystals, and from the crosslinks initially existing in the material. [15,42]With the assumption of an initially homogeneous elastomer network, the first crystals to appear induced a decrease of the elongation of the remaining amorphous phase and a release of latent heat; both phenomena delaying the crystallization kinetics. The second assumption is supported by the fact that, depending on the type of crosslinking, it has been shown that the network created in natural rubber can be more or less heterogeneous[22,43,44]. With this in mind, Candau et al.[22] proposed a model that assumes the presence of several populations of crystallites, each with a different crystallization temperature/elongation couple depending on the local elastically active chain density. The discretization of the crystallites into different populations was based on the evolution of size of the crystals with elongation. The crystals were supposed to reach their final size instantaneously, and the size of the crystal was supposed to be linked to the local

EAC. Figure 6 recalls the $T_c(\lambda)$ curves of varying crystallite populations calculated by Candau for a material very similar to the one of the present study (crosslinked with sulfur and with a similar elastically active chain density). On the same curve, we reported the maximum temperature reached during adiabatic strain, for different values of $\lambda_{max,}$ up to 6.5 (black dotes). One can deduce from this figure that the appearance of the two first populations (green and blue curves) is not inhibited by the generated heat, because their T_c is, for an elongation above 5, higher than the temperature of the sample (black curve). Conversely, for crystallite populations formed by longer chains (low local cross-link density, red curve), the temperature variation reached just after elongation is greater than T_c, which means that the generated heat must first be partially removed for these populations to appear. The duration of the crystallization kinetics is thus extended since the nucleation rate is slowed down due to the time required to decrease the local temperature (i.e., to lower the energetic barrier of nucleation).

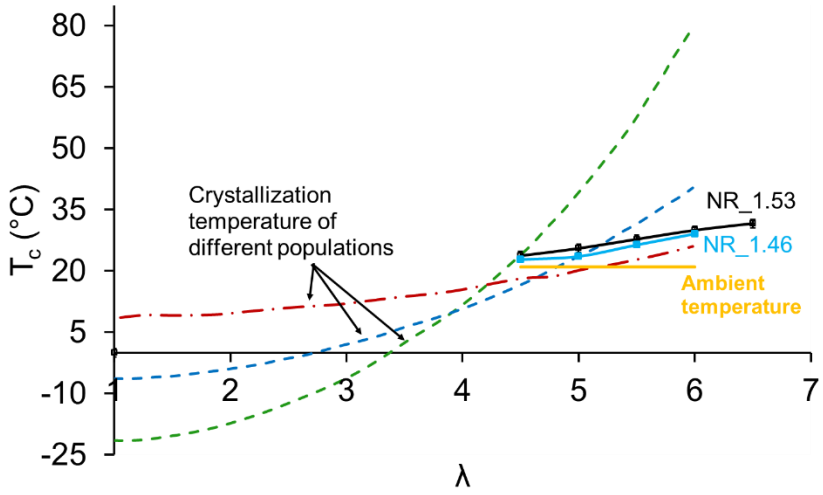

Fig. 6: Crystallization temperature as a function of elongation for different crystallite populations: 1st in green dashed lines, 2nd in blue dashed lines and the 3rd in red dashed lines. The curves were reproduced using equation 10 of the reference [22]. The points represent the maximum temperatures reached by our materials just after stretching at different λ.

4. Conclusion

The majority of the models that describe the crystallization kinetics of NR relate it entirely to the germination, stress relaxation and mobility of the macromolecular chains at a stabilized temperature and do not consider the temperature changes during the cycle. This study highlights the impact of the heat generated by entropic elasticity and crystallization on SIC kinetics and stress relaxation. A difference of at least 10% in the relaxed stress of samples of different thicknesses (200 µm and 1 mm) was observed. It is expected to increase as the

difference in thickness of the samples increases. Consequently, the heat exchange time constant is a parameter that should be considered while modeling SIC and the mechanical behavior of NR. Furthermore, heat transfer could also be partly at the origin of the kinetics of melting of NR crystallites mentioned in the work of Samaca Martinez et al.[27]. Further studies would be needed to confirm it.

In view of being applied to elastocaloric devices[45], these results confirm that a non-negligible crystallization occurs during a few tens of seconds during the heat transfer. In addition, the interplay between stress, temperature and the kinetics of the strain-induced crystallization is believed to have a great impact on the mechanical losses of natural rubber and thus on its coefficient of performance (COP), especially in the case of non-uniform temperature as for regenerative elastocaloric devices (typically when using a liquid as a heat transfer fluid leading to a Biot number above 1). Further work is however necessary to evaluate the impact of non-homogenous crystallization and temperature on the mechanical behavior. It also leads to questions about the impact of the conductive heat diffusion on the crystallization at microscopic and low time scales [46], since the local temperature variation induced by crystallization can reach $\Delta T=\frac{\Delta H_f}{C_m}$=38°C[47].

Finally, from a more general point of view, the high toughness of natural rubber and its dynamic mechanical response are strongly dependent on its ability to crystallize. Consequently, the increase in heat transfer could accelerate the kinetics of SIC and have a significant influence on its fatigue resistance in a marine environment (with a high convective heat transfer coefficient)[48–50]. The dependence of the SIC kinetics on temperature and heat transfer could also be taken into account when investigating crystallization at the crack tip where heat exchange is very specific.

Acknowledgement

This work was supported by ANR (French National Research Agency): ANR-17-CED05-0016, ECPOR project. We would like to thank to French government for funding this research. We also acknowledge the European Synchrotron Radiation Facility (ESRF) for providing the necessary beam-time and the beam-line staff for their guidance during the experiments on the D2AM line. We also thank the ANR for funding the WOS detector on the BM02 beamline (ANR-11-EQPX-0010). Finally, we are grateful to Frédéric Defromerie, Véronique Perrin and Laurence Seveyrat for their technical assistance.

References

[1] A. Chauhan, S. Patel, R. Vaish, C.R. Bowen, A review and analysis of the elasto-caloric effect for solid-state refrigeration devices: Challenges and opportunities, MRS Energy Sustain. 2 (2015) E16. https://doi.org/10.1557/mre.2015.17.

[2] R. Wang, S. Fang, Y. Xiao, E. Gao, N. Jiang, Y. Li, L. Mou, Y. Shen, W. Zhao, S. Li, A.F. Fonseca, D.S. Galvão, M. Chen, W. He, K. Yu, H. Lu, X. Wang, D. Qian, A.E. Aliev, N. Li, C.S. Haines, Z. Liu, J. Mu, Z. Wang, S. Yin, M.D. Lima, B. An, X. Zhou, Z. Liu, R.H. Baughman, Torsional refrigeration by twisted, coiled, and supercoiled fibers, Science (80-.). 366 (2019) 216–221. https://doi.org/10.1126/science.aax6182.

[3] Z. Xie, G. Sebald, D. Guyomar, Comparison of elastocaloric effect of natural rubber with other caloric effects on different-scale cooling application cases, Appl. Therm. Eng. 111 (2017) 914–926. https://doi.org/10.1016/j.applthermaleng.2016.09.164.

[4] S.L. Dart, R.L. Anthony, E. Guth, Rise of Temperature on Fast Stretching of Synthetics and Natural Rubbers, Ind. Eng. Chem. 34 (1942) 1340–1342. https://doi.org/10.1021/ie50395a020.

[5] J.C. Mitchell, D.J. Meier, Rapid Stress-Induced Crystallization in Natural Rubber, Rubber Chem. Technol. 42 (1969) 1420–1432. https://doi.org/10.5254/1.3539309.

[6] Z. Xie, C. Wei, D. Guyomar, G. Sebald, Validity of Flory's model for describing equilibrium strain-induced crystallization (SIC) and thermal behavior in natural rubber, Polymer (Guildf). 103 (2016) 41–45. https://doi.org/10.1016/j.polymer.2016.09.038.

[7] J.-B. Le Cam, A. Tayeb, S. Charlès, First evidence and characterization of strain-induced crystallization heterogeneity in natural rubber under homogeneous strain states, Polymer (Guildf). 255 (2022) 125120. https://doi.org/10.1016/j.polymer.2022.125120.

[8] N. Candau, E. Vives, A.I. Fernández, M.L. Maspoch, Elastocaloric effect in vulcanized natural rubber and natural/wastes rubber blends, Polymer (Guildf). 236 (2021) 124309. https://doi.org/10.1016/j.polymer.2021.124309.

[9] G. Coativy, H. Haissoune, L. Seveyrat, G. Sebald, L. Chazeau, J.-M. Chenal, L. Lebrun, Elastocaloric properties of thermoplastic polyurethane, Appl. Phys. Lett. 117 (2020) 193903. https://doi.org/10.1063/5.0023520.

[10] A. Lachhab, E. Robin, J.-B. Le Cam, F. Mortier, Y. Tirel, F. Canevet, Thermomechanical analysis of polymeric foams subjected to cyclic loading: Anelasticity, self-heating and strain-induced crystallization, Polymer (Guildf). 126 (2017) 19–28. https://doi.org/10.1016/j.polymer.2017.08.010.

[11] R. Bennacer, B. Liu, M. Yang, A. Chen, Refrigeration performance and the elastocaloric effect in natural and synthetic rubbers, Appl. Therm. Eng. 204 (2022) 117938. https://doi.org/10.1016/j.applthermaleng.2021.117938.

[12] S. Zhang, Q. Yang, C. Li, Y. Fu, H. Zhang, Z. Ye, X. Zhou, Q. Li, T. Wang, S. Wang, W. Zhang, C. Xiong, Q. Wang, Solid-state cooling by elastocaloric polymer with uniform chain-lengths, Nat. Commun. 13 (2022) 9. https://doi.org/10.1038/s41467-021-27746-y.

[13] K. Brüning, K. Schneider, S. V. Roth, G. Heinrich, Kinetics of strain-induced

crystallization in natural rubber: A diffusion-controlled rate law, Polymer (Guildf). 72 (2015) 52–58. https://doi.org/10.1016/j.polymer.2015.07.011.

[14] K. Brüning, K. Schneider, S. V. Roth, G. Heinrich, Kinetics of Strain-Induced Crystallization in Natural Rubber Studied by WAXD: Dynamic and Impact Tensile Experiments, Macromolecules. 45 (2012) 7914–7919. https://doi.org/10.1021/ma3011476.

[15] P. Sotta, P.-A. Albouy, Strain-Induced Crystallization in Natural Rubber: Flory's Theory Revisited, Macromolecules. 53 (2020) 3097–3109. https://doi.org/10.1021/acs.macromol.0c00515.

[16] J.C. Mitchell, D.J. Meier, Rapid stress-induced crystallization in natural rubber, J. Polym. Sci. Part A-2 Polym. Phys. 6 (1968) 1689–1703. https://doi.org/10.1002/pol.1968.160061001.

[17] N. Candau, L. Chazeau, J. Chenal, C. Gauthier, J. Ferreira, E. Munch, C. Rochas, Characteristic time of strain induced crystallization of crosslinked natural rubber, Polymer (Guildf). 53 (2012) 2540–2543. https://doi.org/10.1016/j.polymer.2012.04.027.

[18] P.-A. Albouy, G. Guillier, D. Petermann, A. Vieyres, O. Sanseau, P. Sotta, A stroboscopic X-ray apparatus for the study of the kinetics of strain-induced crystallization in natural rubber, Polymer (Guildf). 53 (2012) 3313–3324. https://doi.org/10.1016/j.polymer.2012.05.042.

[19] S. Toki, I. Sics, B.S. Hsiao, M. Tosaka, S. Poompradub, Y. Ikeda, S. Kohjiya, Probing the Nature of Strain-Induced Crystallization in Polyisoprene Rubber by Combined Thermomechanical and In Situ X-ray Diffraction Techniques, Macromolecules. 38 (2005) 7064–7073. https://doi.org/10.1021/ma050465f.

[20] P.-A. Albouy, P. Sotta, Draw Ratio at the Onset of Strain-Induced Crystallization in Cross-Linked Natural Rubber, Macromolecules. 53 (2020) 992–1000. https://doi.org/10.1021/acs.macromol.9b01957.

[21] M. Tosaka, K. Senoo, K. Sato, M. Noda, N. Ohta, Detection of fast and slow crystallization processes in instantaneously-strained samples of cis-1,4-polyisoprene, Polymer (Guildf). 53 (2012) 864–872. https://doi.org/10.1016/j.polymer.2011.12.035.

[22] N. Candau, R. Laghmach, L. Chazeau, J.-M. Chenal, C. Gauthier, T. Biben, E. Munch, Temperature dependence of strain-induced crystallization in natural rubber: On the presence of different crystallite populations, Polymer (Guildf). 60 (2015) 115–124. https://doi.org/10.1016/j.polymer.2015.01.029.

[23] B. Zhao, N. Tian, Y. Liu, T. Yan, W. Zhou, L. Li, Y. Zhou, G. Weng, G. Huang, Strain-induced crystallization of natural rubber with high strain rates, J. Polym. Sci. Part B Polym. Phys. 50 (2012) 1630–1637. https://doi.org/10.1002/polb.23172.

[24] Y.-L. Loo, R.A. Register, A.J. Ryan, Polymer Crystallization in 25-nm Spheres, Phys. Rev. Lett. 84 (2000) 4120–4123. https://doi.org/10.1103/PhysRevLett.84.4120.

[25] Z. Xie, G. Sebald, D. Guyomar, Temperature dependence of the elastocaloric effect in natural rubber, Phys. Lett. A. 381 (2017) 2112–2116. https://doi.org/10.1016/j.physleta.2017.02.014.

[26] P.H. Mott, C.B. Giller, D. Fragiadakis, D.A. Rosenberg, C.M. Roland, Deformation of

443 polyurea: Where does the energy go?, Polym. (United Kingdom). 105 (2016) 227–233.
444 https://doi.org/10.1016/j.polymer.2016.10.029.

445 [27] J.R. Samaca Martinez, J.-B. Le Cam, X. Balandraud, E. Toussaint, J. Caillard,
446 Mechanisms of deformation in crystallizable natural rubber. Part 2: Quantitative
447 calorimetric analysis, Polymer (Guildf). 54 (2013) 2727–2736.
448 https://doi.org/10.1016/j.polymer.2013.03.012.

449 [28] J. Rault, J. Marchal, P. Judeinstein, P.A. Albouy, Chain orientation in natural rubber,
450 Part II: 2H-NMR study, Eur. Phys. J. E. 21 (2006) 243–261.
451 https://doi.org/10.1140/epje/i2006-10064-6.

452 [29] J.-B. Le Cam, P.-A. Albouy, S. Charlès, Comparison between x-ray diffraction and
453 quantitative surface calorimetry based on infrared thermography to evaluate strain-
454 induced crystallinity in natural rubber, Rev. Sci. Instrum. 91 (2020) 044902.
455 https://doi.org/10.1063/1.5141851.

456 [30] P.J. Flory, J. Rehner, Statistical Mechanics of Cross-Linked Polymer Networks I.
457 Rubberlike Elasticity, J. Chem. Phys. 11 (1943) 512–520.
458 https://doi.org/10.1063/1.1723791.

459 [31] B. Heuwers, D. Quitmann, R. Hoeher, F.M. Reinders, S. Tiemeyer, C. Sternemann, M.
460 Tolan, F. Katzenberg, J.C. Tiller, Stress-Induced Stabilization of Crystals in Shape
461 Memory Natural Rubber, Macromol. Rapid Commun. 34 (2012) 180–184.
462 http://doi.wiley.com/10.1002/marc.201200594%0Apapers3://publication/doi/10.1002/
463 marc.201200594.

464 [32] B. Heuwers, A. Beckel, A. Krieger, F. Katzenberg, J.C. Tiller, Shape-memory natural
465 rubber: An exceptional material for strain and energy storage, Macromol. Chem. Phys.
466 214 (2013) 912–923. https://doi.org/10.1002/macp.201200649.

467 [33] M. Tosaka, E. Shigeki, Triaxially oriented shape memory natural rubber, Polymer
468 (Guildf). 157 (2018) 151–155. https://doi.org/10.1016/j.polymer.2018.10.038.

469 [34] J. Chenal, L. Chazeau, L. Guy, Y. Bomal, C. Gauthier, Molecular weight between
470 physical entanglements in natural rubber : A critical parameter during strain-induced
471 crystallization, 48 (2007) 1042–1046. https://doi.org/10.1016/j.polymer.2006.12.031.

472 [35] Y. Yoshida, K. Yuse, D. Guyomar, J.-F. Capsal, G. Sebald, Elastocaloric effect in
473 poly(vinylidene fluoride-trifluoroethylene-chlorotrifluoroethylene) terpolymer, Appl.
474 Phys. Lett. 108 (2016) 242904. https://doi.org/10.1063/1.4953770.

475 [36] L. Mullins, N.R. Tobin, Stress softening in rubber vulcanizates. Part I. Use of a strain
476 amplification factor to describe the elastic behavior of filler-reinforced vulcanized
477 rubber, J. Appl. Polym. Sci. 9 (1965) 2993–3009.
478 https://doi.org/10.1002/app.1965.070090906.

479 [37] R.C. Kerschbaumer, S. Stieger, M. Gschwandl, T. Hutterer, M. Fasching, B. Lechner,
480 L. Meinhart, J. Hildenbrandt, B. Schrittesser, P.F. Fuchs, G.R. Berger, W.
481 Friesenbichler, Comparison of steady-state and transient thermal conductivity testing
482 methods using different industrial rubber compounds, Polym. Test. 80 (2019) 106121.
483 https://doi.org/10.1016/j.polymertesting.2019.106121.

484 [38] V.N. Khiêm, J.-B. Le Cam, S. Charlès, M. Itskov, Thermodynamics of strain-induced
485 crystallization in filled natural rubber under uni- and biaxial loadings, Part I: Complete

energetic characterization and crystallinity evaluation, J. Mech. Phys. Solids. 159 (2022) 104701. https://doi.org/10.1016/j.jmps.2021.104701.

[39] J. Plagge, M. Klüppel, Determining strain-induced crystallization of natural rubber composites by combined thermography and stress-strain measurements, Polym. Test. 66 (2018) 87–93. https://doi.org/10.1016/j.polymertesting.2017.12.021.

[40] L.A. Wood, G.M. Martin, Compressibility of natural rubber at pressures below 500 kg/cm2, J. Res. Natl. Bur. Stand. Sect. A Phys. Chem. 68A (1964) 259. https://doi.org/10.6028/jres.068A.022.

[41] P.J. Flory, Thermodynamics of Crystallization in High Polymers. I. Crystallization Induced by Stretching, J. Chem. Phys. 15 (1947) 397–408. https://doi.org/10.1063/1.1746537.

[42] B. Huneau, STRAIN-INDUCED CRYSTALLIZATION OF NATURAL RUBBER: A REVIEW OF X-RAY DIFFRACTION INVESTIGATIONS, Rubber Chem. Technol. 84 (2011) 425–452. https://doi.org/10.5254/1.3601131.

[43] M. Wirtz, R. Rommel, J. López Valentín, S. Westermann, F. Sportelli, F. Kayser, Solvents for thermoporosimetry analysis of natural rubber networks, J. Appl. Polym. Sci. 133 (2016). https://doi.org/10.1002/app.43998.

[44] J.L. Valentín, J. Carretero-González, I. Mora-Barrantes, W. Chassé, K. Saalwächter, Uncertainties in the Determination of Cross-Link Density by Equilibrium Swelling Experiments in Natural Rubber, Macromolecules. 41 (2008) 4717–4729. https://doi.org/10.1021/ma8005087.

[45] G. Sebald, A. Komiya, J. Jay, G. Coativy, L. Lebrun, Regenerative cooling using elastocaloric rubber: Analytical model and experiments, J. Appl. Phys. 127 (2020) 094903. https://doi.org/10.1063/1.5132361.

[46] A.A. Minakov, C. Schick, Nanometer scale thermal response of polymers to fast thermal perturbations, J. Chem. Phys. 149 (2018) 074503. https://doi.org/10.1063/1.5044187.

[47] V.N. Khiêm, M. Itskov, Analytical network-averaging of the tube model: Strain-induced crystallization in natural rubber, J. Mech. Phys. Solids. 116 (2018) 350–369. https://doi.org/10.1016/j.jmps.2018.04.003.

[48] K. Narynbek Ulu, B. Huneau, P.-Y. Le Gac, E. Verron, Fatigue resistance of natural rubber in seawater with comparison to air, Int. J. Fatigue. 88 (2016) 247–256. https://doi.org/10.1016/j.ijfatigue.2016.03.033.

[49] P.-Y. Le Gac, M. Arhant, P. Davies, A. Muhr, Fatigue behavior of natural rubber in marine environment: Comparison between air and sea water, Mater. Des. 65 (2015) 462–467. https://doi.org/10.1016/j.matdes.2014.09.032.

[50] P. Kosky, R. Balmer, W. Keat, G. Wise, Mechanical Engineering, in: Explor. Eng., Elsevier, 2021: pp. 317–340. https://doi.org/10.1016/B978-0-12-815073-3.00014-4.